Available online at www.sciencedirect.com
SCIENCE DIRECT®
Journal of Solid State Chemistry 170 (2003) 142–153
JOURNAL OF SOLID STATE CHEMISTRY
http://elsevier.com/locate/jssc

An evaluation of silver ionic transport in the mixed system $(1-x)\cdot CuI–x\cdot Ag_2MoO_4$ $(0.15\leqslant x\leqslant 0.6)$

S. Austin Suthanthiraraj* and Y. Daniel Premchand

Department of Energy, School of Energy and Material Sciences, University of Madras, Guindy Campus, Chennai 600 025, India

Received 3 June 2002; received in revised form 29 August 2002; accepted 12 September 2002

Abstract

The origin and nature of correlation between silver ionic conduction and composition of various phases present in the case of the mixed system $CuI–Ag_2MoO_4$ were probed in terms of possible solid-state reactions. Detailed X-ray diffraction (XRD), differential scanning calorimetry, Fourier transform infrared, electrical transport studies involving ionic transport number data and electrical conductivity measurement were carried out in order to identify the reaction products. The feasible reaction products identified were found to determine the exact composition resulting from the completion of each solid-state reaction and hence the behavior of effective electric conduction.

Keywords: Solid-state reaction; Electrical conductivity; Silver ionic conduction

1. Introduction

Studies pertaining to the development of fast ion conducting solids have been carried out extensively, because of their potential application as solid electrolytes in high energy density batteries [1]. In recent years, our research group has developed a new class of solid electrolytes exhibiting appreciably high silver ion conductivity values in several mixed systems involving CuI and silver oxyacid salts through a systematic study of their electrical and electrochemical properties [2–6]. However, a careful evaluation of the application prospects of such solid electrolyte systems appears to emphasize the need for a better understanding of the origin and nature of effective electric conduction. In fact, this may be achieved only through the knowledge of composition and relevant properties of the reaction products formed as a result of probable solid-state reactions occurring between CuI and the corresponding silver oxyacid salt. Accordingly, the present study involves a systematic evaluation of effective electric conduction in the mixed system $(1-x)\cdot CuI–x\cdot Ag_2MoO_4$, where $0.15\leqslant x\leqslant 0.6$ through the solid-state reaction route and an unambiguous interpretation relating the observed silver ionic conduction to the composition of the constituent mixtures.

2. Experimental

Commercially available analar grade cuprous iodide (CuI) and freshly prepared silver molybdate (Ag_2MoO_4) were used as starting materials. Silver molybdate was initially precipitated from an aqueous solution of $AgNO_3$ and Na_2MoO_4 under safelight conditions. The fresh precipitate was filtered and dried at 373 K in a vacuum oven. Various samples of the mixed system $(1-x)\cdot CuI–x\cdot Ag_2MoO_4$, where $x=0.15$, 0.2, 0.25, 0.3,0.33, 0.35, 0.4, 0.45, 0.5, 0.55 and 0.6, respectively, were then synthesized by standard melt quenching method. Appropriate amounts of CuI and Ag_2MoO_4 were mixed, grounded together, sealed in Pyrex tubes under vacuum and annealed at 773 K for 30 min before being quenched in liquid nitrogen. Solid samples thus obtained were designated as Series I (representing those compositions having $x=0.15$, 0.2, 0.25, 0.3 and 0.33) and Series II (corresponding to those samples with $x=$ 0.35, 0.4, 0.45, 0.5, 0.55 and 0.6), respectively, and used for further studies.

*Corresponding author. Fax: +91-44-2350305.
E-mail address: suthan98@yahoo.com (S.A. Suthanthiraraj).

0022-4596/03/$ - see front matter © 2002 Elsevier Science (USA). All rights reserved.
PII: S0022-4596(02)00047-6

The crystalline nature of these samples and their identity were examined by powder X-ray diffraction (XRD) analysis. The room temperature XRD patterns were obtained using a Siefert X-ray diffractometer with Cu$K\alpha 1$ radiation ($\lambda = 1.541$ Å). Differential scanning calorimetric (DSC) experiments were carried out on all the samples using a Perkin-Elmer Model DSC-7 calorimeter over the temperature range 323–773 K at a heating rate of 20°C/min under nitrogen atmosphere. Fourier transform infrared (FT-IR) absorption spectra in the 400–1200 cm^{-1} range were recorded for the above specimens on a Burger IFS66 V FT-IR spectrometer.

Electrical conductivity (σ) measurements were carried out by the complex impedance method on pellet samples of 8 mm diameter sandwiched between a pair of silver electrodes using a Hewlett-Packard (model HP 4284A) Precision LCR meter in the frequency range 20–1 MHz and over the temperature range 297–447 K. The complex impedance analysis was employed for the extraction of bulk resistance values and separation of electrode and grain-boundary components from the experimental data as outlined below:

As superionic conductors or solid electrolytes are mostly studied in the form of polycrystalline specimens, grain-boundary impedances are known to influence the evaluation of their bulk conductivity values. Accordingly, the analysis of bulk properties and separation of grain-boundary as well as electrode–electrolyte interfacial effects are not simple and the selection of appropriate equivalent circuit is also difficult due to inhomogenities within the bulk sample, which make the observed bulk impedance frequency dependant [7,8]. For the sake of clarity, a schematic representation of a polycrystalline superionic solid sandwiched between two non-blocking (i.e., reversible) electrodes together with the relevant equivalent circuit and impedance plot is shown in Fig. 1.

According to Macdonald [9] such a complex impedance plot drawn over a range of frequencies would consist of three arcs including a high frequency one, which is associated with the bulk conductivity (due to the electrolytic resistance, R_b) shunted by the geometric capacitance 'C_g' (capacitative coupling between the electrodes), whereas the arc of intermediate frequencies shows the effect of the geometric capacity C_g and the impedance double-layer capacitance 'C_{dl}' associated with the charge transfer (charging and discharging at the electrode/electrolyte interface) processes. On the other hand, the low-frequency arc is generally inclined at an angle of $\sim 45°$ to the real axis and is specifically attributed to Z_d, the impedance due to the diffusion process arising from the presence of concentration gradient within the specimen. In the case of practical systems, all these three arcs may not be present or only a part of the arc could be identified. Usually, the behavior of the bulk sample and that of the interfacial impedance

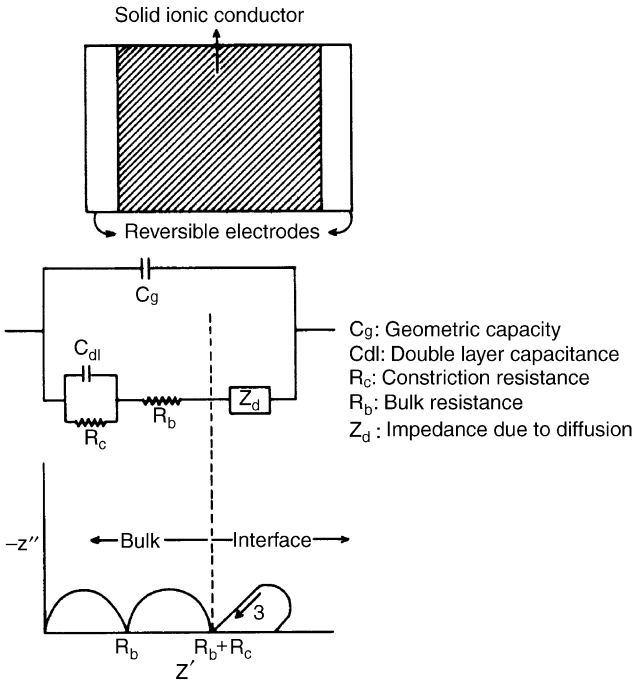

Fig. 1. Schematic representation of a solid ionic conductor held between two reversible electrodes shown with its impedance plot and an equivalent circuit.

are quite different from each other. However, in most of the systems, there is a distinct minimum in Z'' between the two regions as shown in Fig. 1 and the value of Z' at this minimum of Z'' is the best estimate for the overall bulk resistance (including the constriction resistance, R_c between the grains). Extrapolation of the impedance to the higher frequencies in the interface dispersion region or to the lower frequencies in the bulk dispersion region is also known to provide another way of determination of the bulk resistance from the complex impedance plot [10–12].

During the present investigation, the frequency response of a variety of compositions of the chosen system was measured in terms of the real (Z') and imaginary (Z'') parts of the complex impedance (Z^*) at different temperatures. The point of intersection of the impedance plots on the real axis in the high-frequency region was taken as the bulk resistance (R_b) of the sample. The electrical conductivity (σ) of the sample was estimated using the relationship

$$\sigma = t/AR_b, \quad (1)$$

where t is the thickness of the specimen and A is the area of cross-section. Furthermore, a combined analysis of the modulus and impedance spectra over the frequency range of measurement was also carried out for the identification and separation of electrode/electrolyte interfacial effects from the bulk electrical conductivity results.

The EMF method was employed for the estimation of ionic transport number t_i of the specimens [13]. Accordingly, the open-circuit voltage (OCV) values of galvanic cells fabricated with the configuration (−) Ag/Sample/I_2 (+) were compared with the theoretical value of 687 mV for the evaluation of t_i values [14].

3. Results and discussion

3.1. XRD and DSC data

The room temperature powder XRD patterns obtained for five different samples in Series I of the mixed system $(1-x)\cdot CuI–x\cdot Ag_2MoO_4$, where $x = 0.15$, 0.2, 0.25, 0.3 and 0.33, respectively, are shown in Fig. 2. It is interesting to note from Fig. 2(a) that three prominent diffraction peaks, which appear at $2\theta = 24.8°$, 41.1° and 48.6°, respectively, in the case of the typical composition with $x = 0.15$ tend to shift gradually towards lower 2Θ values as the content of Ag_2MoO_4 is increased from $x = 0.15$ to 0.3. Furthermore, these XRD peaks are found to be consistent with those of γ-CuI while being indexed as reflections corresponding to [111], [220] and [311], respectively, on the basis of the face-centered cubic unit cell of the space group $F\bar{4}3m$. The fact that the set of three XRD peaks observed in the case of the composition having $x = 0.33$ are comparable to that of γ-AgI suggest the feasibility of formation of γ-AgI as one of the constituents of this particular composition. It is therefore apparent that continuous solid solutions of the type $Cu_{1-a}Ag_aI$ between ionic salts such as CuI and AgI may be formed in the specimens of Series I as the value of x is increased from $x = 0.15$ to 0.33. In the case of $Cu_{1-a}Ag_aI$ solid solutions the lattice parameter was reported to obey the so-called Vegard's law [15]. This means that the composition dependence of the positions of the diffraction lines (i.e., d-spacings) of $Cu_{1-a}Ag_aI$ solid solutions is generally linear, where 'a' refers to the atomic fraction of silver content within the specimen.

Fig. 3 represents the variation of the lattice parameter [1] of the typical solid solution $Cu_{1-a}Ag_aI$ as a function of composition estimated in accordance with Vegard's law by considering the lattice parameters of the terminal phases namely CuI and AgI as well [16]. It is obvious from Fig. 3 that the lattice parameter varies linearly with the silver content. From the present XRD results obtained for the chosen compositions of Series I namely those having $x = 0.15$, 0.2, 0.25, 0.3 and 0.33 the estimated values of their respective lattice parameters on the basis of the face-centered cubic unit cell are 6.2, 6.28, 6.4, 6.44 and 6.5 Å. Fig. 3 appears to suggest that the most probable stoichiometry of $Cu_{1-a}Ag_aI$ solid solutions present in five different compositions with $x = 0.15$, 0.2, 0.25, 0.3 and 0.33 may be expressed as

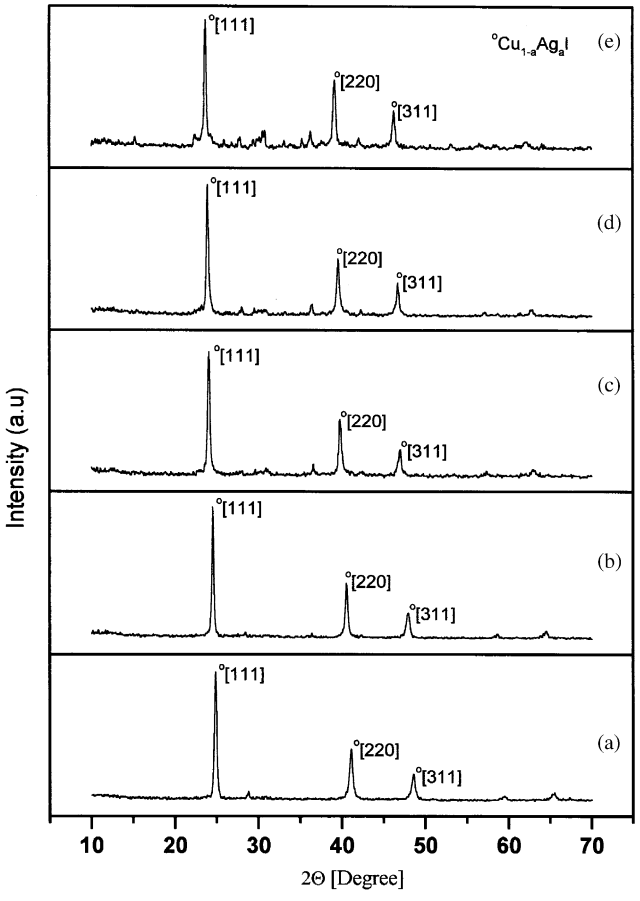

Fig. 2. Powder X-ray diffraction patterns for samples in Series I of the mixed system $(1-x)\cdot CuI–x\cdot Ag_2MoO_4$: (a) $x = 0.15$; (b) $x = 0.2$; (c) $x = 0.25$; (d) $x = 0.3$ and (e) $x = 0.33$.

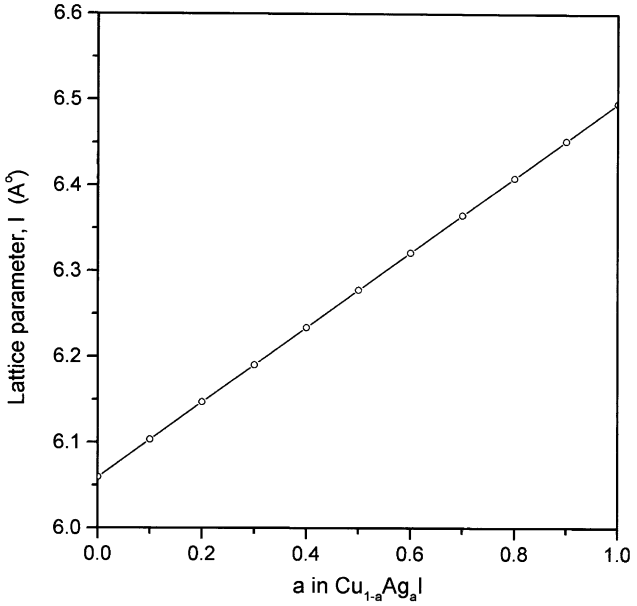

Fig. 3. Vegard's law behavior of the lattice parameter of $Cu_{1-a}Ag_aI$ solid solution ($0 \leqslant a \leqslant 1$).

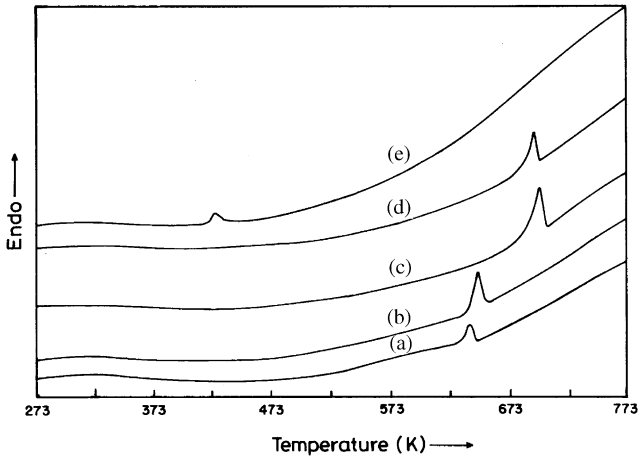

Fig. 4. DSC thermograms for samples in Series I of the mixed system $(1-x)\cdot CuI–x\cdot Ag_2MoO_4$: (a) $x=0.15$; (b) $x=0.2$; (c) $x=0.25$; (d) $x=0.3$ and (e) $x=0.33$.

$Cu_{0.68}Ag_{0.32}I$, $Cu_{0.5}Ag_{0.5}I$, $Cu_{0.25}Ag_{0.75}I$, $Cu_{0.14}Ag_{0.86}I$, and AgI, respectively.

Fig. 4 depicts the DSC thermograms recorded for the five different samples in Series I of the mixed system $(1-x)\cdot CuI–x\cdot Ag_2MoO_4$, where $x=0.15$, 0.20, 0.25, 0.30 and 0.33, respectively. It is clear from Fig. 4 that endothermic peaks are observed at 638, 646, 698, 693 and 423 K, respectively, in the above compositions. In view of the fact CuI undergoes a phase transition from its γ-phase into the β-phase at 642 K, the endothermic peaks noticed at 638 and 646 K in the case of compositions having $x=0.15$ and 0.2 may be attributed to the $\gamma-\beta$ phase transition temperature of the CuI–AgI solid solutions present within these specimens [17]. On the other hand, the appearance of an endothermic peak at 423 K in the case of the particular sample having $x=0.33$ may be attributed to the $\beta-\alpha$ phase transition temperature of AgI. Therefore, the formation of solid solutions of the type $Cu_{1-a}Ag_aI$ and assignment of their stoichiometry on the basis of the observed XRD results are found to be in good agreement with the present DSC data as well.

Fig. 5 indicates the room temperature powder XRD patterns observed for six different samples in Series II of the mixed system $(1-x)\cdot CuI–x\cdot Ag_2MoO_4$ having $x=$ 0.35, 0.4, 0.45, 0.5, 0.55 and 0.6, respectively. A careful examination of Fig. 5 suggests that the number of XRD peaks increases as the value of x is increased from 0.35 to 0.6 and that the set of three prominent peaks (marked °) corresponding to the respective reflection lines of [111], [220] and [311] planes may be attributed to the presence of γ-AgI in all the specimens. Furthermore, in the case of Figs. 5(b)–(f) it is seen that a typical peak (marked *) due to the presence of metallic silver also appears. All the remaining XRD peaks noticed in Fig. 5 (marked !) may be ascribed to the formation of a new

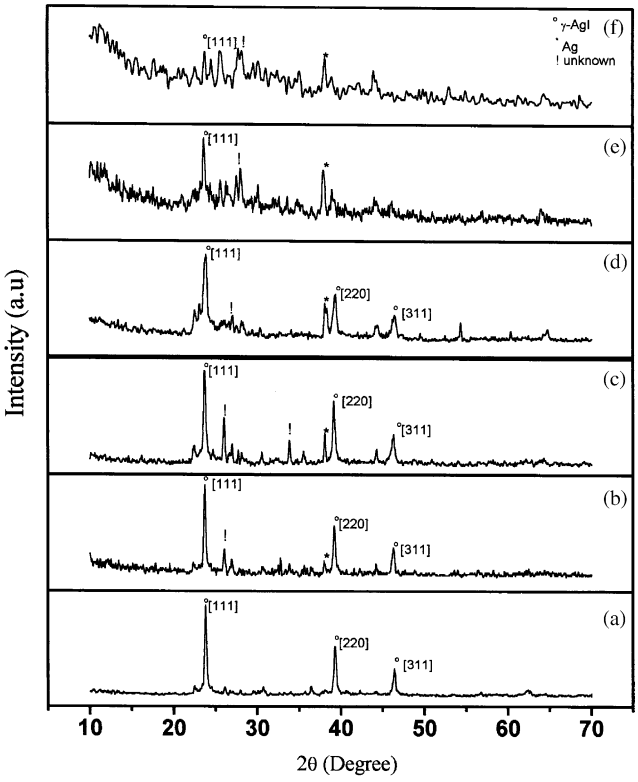

Fig. 5. Powder X-ray diffraction patterns for samples in Series II of the mixed system $(1-x)\cdot CuI–x\cdot Ag_2MoO_4$: (a) $x=0.35$; (b) $x=0.4$; (c) $x=0.45$; (d) $x=0.5$; (e) $x=0.55$ and (f) $x=0.6$.

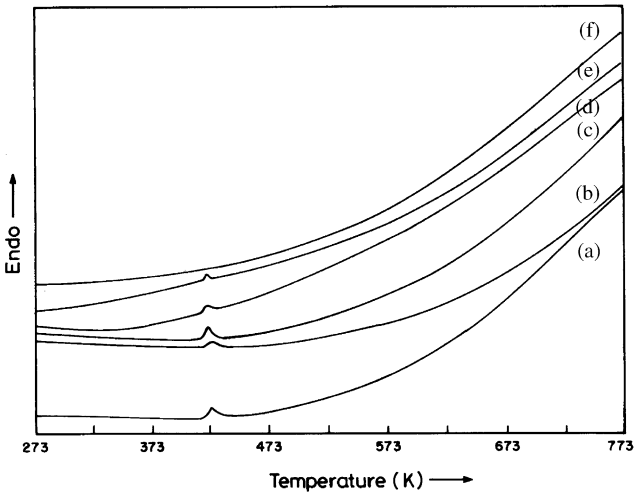

Fig. 6. DSC thermograms for samples in Series II of the mixed system $(1-x)\cdot CuI–x\cdot Ag_2MoO_4$: (a) $x=0.35$; (b) $x=0.4$; (c) $x=0.45$; (d) $x=0.5$; (e) $x=0.55$ and (f) $x=0.6$.

crystalline phase along with γ-AgI and metallic silver. Fig. 6 shows the DSC thermograms recorded for the six different specimens of Series II of the mixed system having $x=0.35$, 0.4, 0.45, 0.5, 0.55 and 0.6, respectively. It may be noticed from Fig. 6 that endothermic peaks

appear at 423, 423, 421 and 420 K in the case of samples having $x = 0.35$, 0.4, 0.45 and 0.5, respectively, the values of which are comparable to the $\beta-\alpha$ phase transition temperature of 420 K reported for pure AgI. The non-appearance of an endothermic peak around 420 K in the case of DSC trace for $x = 0.6$ may be attributed to the lower content of AgI in this particular specimen as compared to the remaining compositions of Series II considered during the present investigation.

3.2. FT-IR data

Fig. 7 shows the FT-IR spectra observed for five different compositions in Series I of the mixed system $(1-x)\cdot CuI–x\cdot Ag_2MoO_4$ where $x = 0.15$, 0.2, 0.25, 0.3 and 0.33, respectively, at room temperature. In Fig. 7, the strong absorption bands observed at around 835 cm^{-1} and the shoulder at 914 cm^{-1} may be assigned, respectively, to the ν_3 and ν_1 modes of vibrations of the tetrahedral MoO_4^{2-} ions [18]. On the other hand, the presence of two weak bands at around 628 and 468 cm^{-1} may be ascribed to the Mo–O–Mo bridging arising as a result of the condensation of MoO_4^{2-} ions. It is therefore clear from the FT-IR analysis of Series I that tetrahedral MoO_4^{2-} ions are present in these specimens. Fig. 8 depicts the FT-IR spectra obtained in the case of six different samples in Series II of the mixed system $(1-x)\cdot CuI–x\cdot Ag_2MoO_4$ having $x = 0.35$, 0.4, 0.45, 0.5, 0.55 and 0.6, respectively. On the other hand, Table 1 indicates the positions of the absorption bands observed in these specimens along with their assignments in terms of the various molecular species present. A careful analysis of Fig. 8 in conjugation with Table 1 appears to suggest that in the case of a particular specimen having $x = 0.35$, the absorption band observed at 421 cm^{-1} may be ascribed to the tetrahedral MoO_4^{2-} ions whereas all the remaining bands appearing at 447, 800, 815,917 and 949 cm^{-1} may be attributed to the formation of $Mo_2O_7^{2-}$ ions as in the case of crystalline $Na_2Mo_2O_7$ [19,20].

It is also obvious from Table 1 that in the case of a sample having $x = 0.4$, all the absorption bands at 447, 776, 815, 916 and 947 cm^{-1} may be assigned to the presence of $Mo_2O_7^{2-}$ species. However, the absorption bands at 421 and 423 cm^{-1} in the case of $x = 0.45$ and 0.5, respectively, suggests the presence of tetrahedral MoO_4^{2-} ions whereas those bands appearing at 449, 780, 819, 917 and 947 cm^{-1} as well as those observed at 797, 821, 862, 880 and 948 cm^{-1} may be attributed to the formation of $Mo_2O_7^{2-}$ ions in the above compositions [20]. It is interesting to note from Table 1 that tetrahedral MoO_4^{2-} ions are present as predominant molecular species in the typical samples with $x = 0.55$ and 0.6 in view of the fact that the set of absorption bands appearing at 415, 841, 924 and 966 cm^{-1} in the former and those appearing at 420 and 836 cm^{-1} in the latter may be assigned to the MoO_4^{2-} ions [19]. In the case of $x = 0.55$, the remaining absorption band observed at 880 cm^{-1} tends to suggest the presence of $Mo_2O_7^{2-}$ ions in the sample. The present FT-IR results have thus established the fact that in the case of Series II samples $Mo_2O_7^{2-}$ ions are formed as predominant molecular species in the case of samples with $x = 0.35$, 0.4, 0.45 and 0.5, whereas tetrahedral monomeric MoO_4^{2-} ions constitute the molybdenum-based anionic environment in Ag_2MoO_4 rich specimen having $x =$ 0.55 and 0.6, respectively.

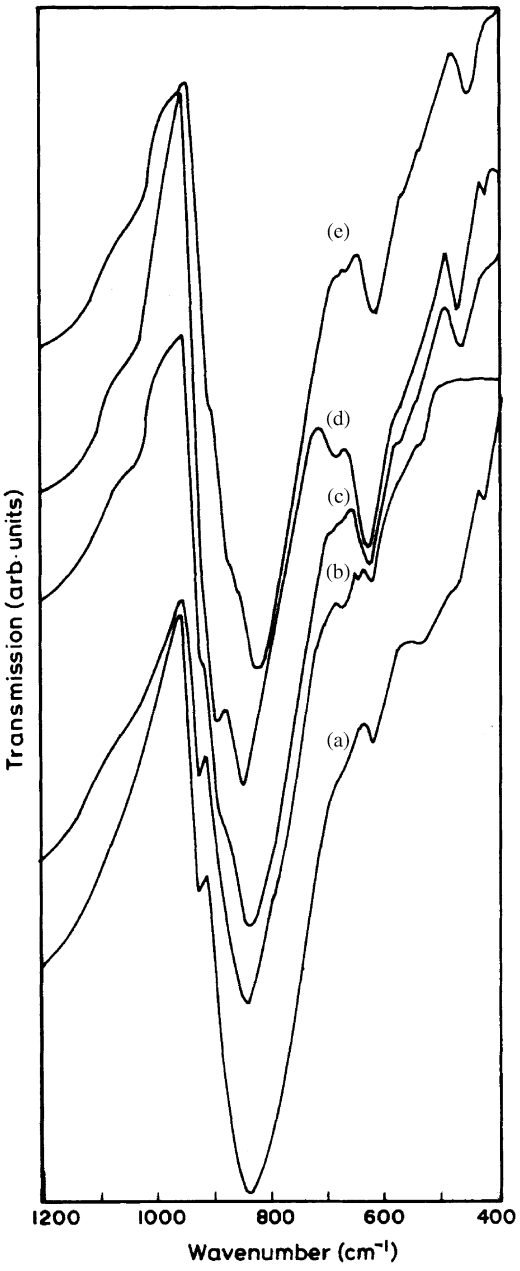

Fig. 7. FT-IR spectra observed for samples in Series I of the mixed system $(1-x)\cdot CuI–x\cdot Ag_2MoO_4$: (a) $x = 0.15$; (b) $x = 0.2$; (c) $x = 0.25$; (d) $x = 0.3$ and (e) $x = 0.33$.

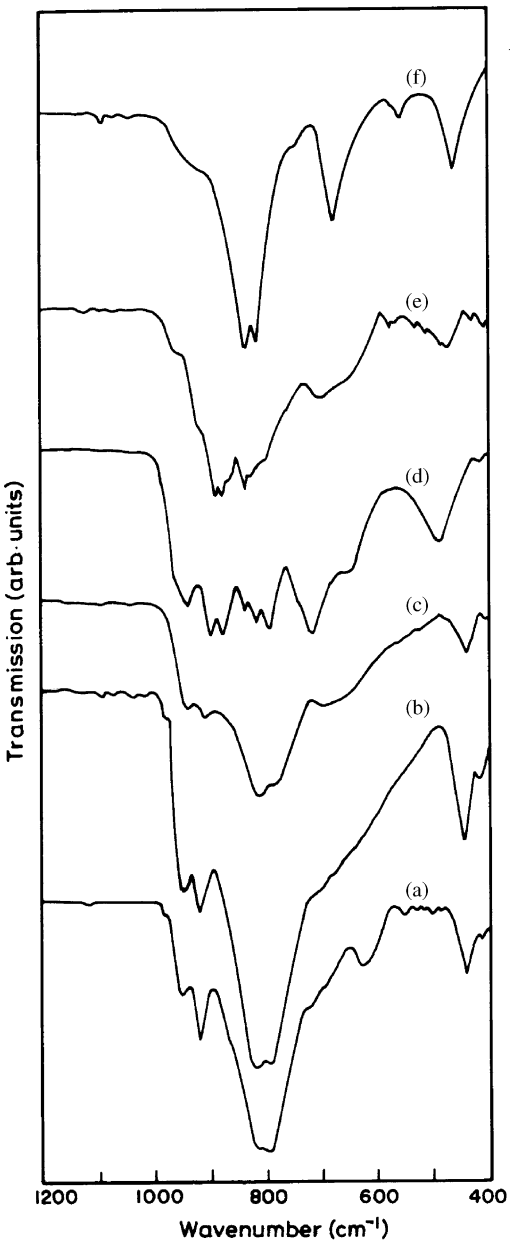

Fig. 8. FT-IR spectra observed for samples in Series II of the mixed system $(1-x)\cdot$CuI–$x\cdot Ag_2MoO_4$: (a) $x=0.35$; (b) $x=0.4$; (c) $x=0.45$; (d) $x=0.5$; (e) $x=0.55$ and (f) $x=0.6$.

Table 1
FT-IR absorption bands observed for various compositions in Series II of the mixed system $(1-x)\cdot$CuI–$x\cdot Ag_2MoO_4$ and their assignments

Composition	Observed absorption band (cm^{-1})	Assignment
0.35	421	MoO_4^{2-}
	447	$Mo_2O_7^{2-}$
	800	$Mo_2O_7^{2-}$
	815	$Mo_2O_7^{2-}$
	917	$Mo_2O_7^{2-}$
	949	$Mo_2O_7^{2-}$
0.4	447	$Mo_2O_7^{2}$
	776	$Mo_2O_7^{2-}$
	815	$Mo_2O_7^{2-}$
	916	$Mo_2O_7^{2-}$
	947	$Mo_2O_7^{2-}$
0.45	421	MoO_4^{2-}
	449	$Mo_2O_7^{2-}$
	780	$Mo_2O_7^{2-}$
	819	$Mo_2O_7^{2-}$
	917	$Mo_2O_7^{2-}$
	947	$Mo_2O_7^{2-}$
0.5	423	MoO_4^{2-}
	797	$Mo_2O_7^{2-}$
	821	$Mo_2O_7^{2-}$
	862	$Mo_2O_7^{2-}$
	880	$Mo_2O_7^{2-}$
	948	$Mo_2O_7^{2-}$
0.55	415	MoO_4^{2-}
	841	MoO_4^{2-}
	880	$Mo_2O_7^{2-}$
	815	$Mo_2O_7^{2-}$
	924	MoO_4^{2-}
	966	MoO_4^{2-}
0.6	420	MoO_4^{2-}
	836	MoO_4^{2-}

3.3. Solid-state reactions

3.3.1. Series I samples

The present XRD, DSC and FT-IR results have indicated the formation of solid solutions of the type $Cu_{1-a}Ag_aI$ ($0\leqslant a\leqslant 1$) as well as another phase consisting of MoO_4^{2-} ions as the anionic species in all the rapidly quenched specimens of Series I of the mixed system $(1-x)\cdot$CuI–$x\cdot Ag_2MoO_4$, where $x=0.15$, 0.2, 0.25, 0.3 and 0.33. In other words, such phases may be obtained as a result of solid-state reactions occurring between the starting materials namely CuI and Ag_2MoO_4 within the melt. Usually, in the case of a reaction between two solid substances $A'X'$ and $A''X''$, if A' and A'' ions are more mobile, there would be a distribution of A' and A'' ions across the boundary of both these phases. As a consequence, A'' ions may diffuse into the lattice of $A'X'$ resulting in the formation of the solid solution $(A', A'')X'$ until the dissolution of A' is complete. Such type of reaction was grouped under Class C in Jost's classification of solid-state reactions [21]. In analogy with these reactions, the most probable solid-state reactions between CuI and Ag_2MoO_4 may be described in the following manner:

(a) $x=0.15$ (CuI/Ag_2MoO_4 molar ratio 17:3):

$$17CuI + 3Ag_2MoO_4 \rightarrow 17Cu_{0.65-\delta}Ag_{0.35+\delta}I + 3Cu_2MoO_4, \quad (2)$$

where $0\leqslant\delta\leqslant 0.01$.

(b) $x=0.2$ (CuI/Ag_2MoO_4 molar ratio 4:1):

$$4CuI + Ag_2MoO_4 \rightarrow 4Cu_{0.5}Ag_{0.5}I + Cu_2MoO_4. \quad (3)$$

(c) $x = 0.25$ (CuI/Ag_2MoO_4 molar ratio 3:1):

$$3CuI + Ag_2MoO_4 \rightarrow 3Cu_{0.25+\tau}Ag_{0.75-\tau}I + Cu_2MoO_4, \quad (4)$$

where $0 \leqslant \tau \leqslant 0.01$.

(d) $x = 0.3$ (CuI/Ag_2MoO_4 molar ratio 7:3):

$$7CuI + 3Ag_2MoO_4 \rightarrow 7Cu_{0.14+\varphi}Ag_{0.86-\varphi}I + 3Cu_2MoO_4, \quad (5)$$

where $0 \leqslant \varphi \leqslant 0.01$.

(e) $x = 0.33$ (CuI/Ag_2MoO_4 molar ratio 2:1):

$$2CuI + Ag_2MoO_4 \rightarrow 2AgI + Cu_2MoO_4. \quad (6)$$

Eqs. (2)–(6) have been proposed on the basis of the reaction products identified from the present XRD and DSC results in the light of FT-IR data. It is also worthwhile to mention that three parameters δ, τ and φ have been incorporated in Eqs. (2)–(5), respectively, in order to account for the stoichiometry of these solid-state reactions. The fact that the various solid solutions of the type $Cu_{1-a}Ag_aI$ shown in Eqs. (2)–(6) are in excellent agreement with those identified form of present XRD results involving lattice parameter of such phases appears to substantiate the proposed solid-state reaction mechanism. Furthermore, the formation of AgI as a reaction product in the case of sample with $x = 0.33$ is also evident from the present XRD and DSC results. Interestingly, the appearance of the anionic species involving MoO_4^{2-} ions identified from the present FI-IR spectral analysis may conveniently be considered as belonging to the additional reaction product namely Cu_2MoO_4 in all the samples of Series I. In the light of these facts, it is reasonable to argue that the proposed solid-state reactions in the case of different compositions of Series I of the chosen system are logical too.

3.3.2. Series II samples

From Section 3.3.1 it is evident that when the value of x is increased from 0.15 to 0.33, the solid solution $Cu_{1-a}Ag_aI$ becomes AgI as confirmed by the XRD and DSC results. Since Series II includes those samples having $x = 0.35$, 0.4, 0.45, 0.5, 0.55 and 0.6, it is reasonable to presume that any further addition of Ag_2MoO_4 in excess of stoichiometric composition (with a CuI/Ag_2MoO_4 molar ratio 2:1) in the molten mixture containing CuI and Ag_2MoO_4 would result in the incorporation of Ag_2MoO_4 (excess) as another reaction product in addition to AgI and Cu_2 MoO_4. In other words, in the case of compositions having $x > 0.33$, the formation of AgI and Cu_2 MoO_4 as probable reaction products may be associated with an additional product namely Ag_2MoO_4 (excess) as well. In this perspective, the set of equations representing the most probable solid-state reaction between CuI and Ag_2MoO_4 in the case of various compositions of Series II may be given as follows:

(f) $x = 0.35$ (CuI/Ag_2MoO_4 molar ratio 13:7):

$$26CuI + 14Ag_2MoO_4 \rightarrow 26AgI + 13Cu_2MoO_4 + Ag_2MoO_4 \text{ (excess)}. \quad (7)$$

(g) $x = 0.40$ (CuI/Ag_2MoO_4 molar ratio 3:2):

$$6CuI + 4Ag_2MoO_4 \rightarrow 6AgI + 3Cu_2MoO_4 + Ag_2MoO_4 \text{ (excess)}. \quad (8)$$

(h) $x = 0.45$ (CuI/Ag_2MoO_4 molar ratio 11:9):

$$22CuI + 18Ag_2MoO_4 \rightarrow 22AgI + 11Cu_2MoO_4 + 7Ag_2MoO_4 \text{ (excess)}. \quad (9)$$

(i) $x = 0.5$ (CuI/Ag_2MoO_4 molar ratio 1:1):

$$2CuI + 2Ag_2MoO_4 \rightarrow 2AgI + Cu_2MoO_4 + Ag_2MoO_4 \text{ (excess)}. \quad (10)$$

(j) $x = 0.55$ (CuI/Ag_2MoO_4 molar ratio 9:11):

$$18CuI + 22Ag_2MoO_4 \rightarrow 18AgI + 9Cu_2MoO_4 + 13Ag_2MoO_4 \text{ (excess)}. \quad (11)$$

(k) $x = 0.6$ (CuI/Ag_2MoO_4 molar ratio 2:3):

$$2CuI + 3Ag_2MoO_4 \rightarrow 2AgI + Cu_2MoO_4 + 2Ag_2MoO_4 \text{ (excess)}. \quad (12)$$

Eqs. (7)–(12) are found to be in good agreement with the present XRD, DSC and FT-IR results in view of the fact the presence of AgI in all the six different compositions in Series II of the mixed system $(1-x)\cdot CuI$–$x\cdot Ag_2MoO_4$ has already been detected during the XRD analysis. The present DSC analysis has also reconfirmed the presence of AgI in most of these samples. However, it is apparent that the present XRD results have indicated the presence of certain other additional phases. A precise identification of each of these new phases could not be carried out from the XRD data owing to the weak and diffused nature of the observed XRD patterns. Interestingly, one of the significant results of the present investigation has been the identification of suitable solid-state reaction between CuI and Ag_2MoO_4 as a function of composition and possible mechanisms. In this regard, further studies concerning the transport features of the various compositions would throw more light as discussed in the forthcoming section.

3.4. Electrical conductivity results

Fig. 9 depicts the complex impedance plots obtained for the typical composition corresponding to $x = 0.2$ in the system $(1-x)\cdot CuI$–$x\cdot Ag_2MoO_4$ at four different temperatures namely 297, 315, 330 and 345 K, respectively. It is obvious from Fig. 9 that the diameter of the semicircle decreases as the temperature is raised from 297 to 345 K. This means that the point of intersection of the impedance plot on the real axis (i.e., Z'-axis),

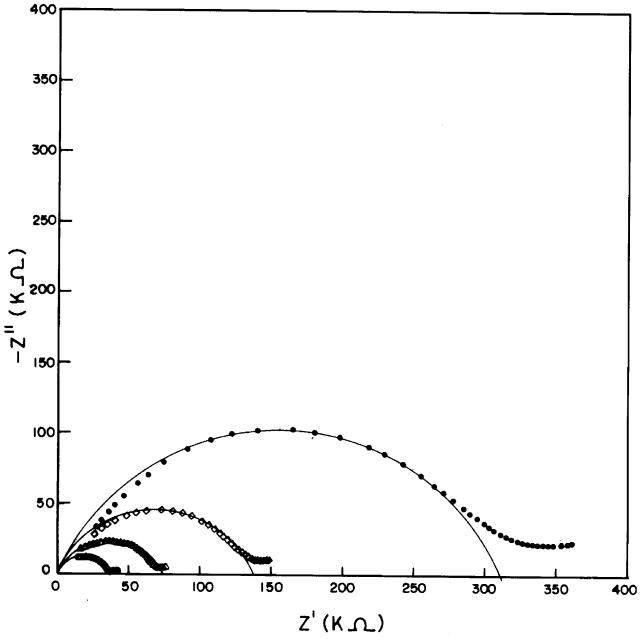

Fig. 9. Complex impedance plots obtained for the typical composition having $x = 0.2$ in the system $(1-x)\cdot CuI$–$x\cdot Ag_2MoO_4$ at different temperatures: $T = 297\,K$ (●); 315 K (◇); 330 K (△) and 345 K (○).

which denotes the bulk resistance R_b of the sample decreases at elevated temperature. In other words, the observed electrical conductivity (σ) would tend to increase with increasing temperature as in the case of ionic solids. Similar patterns have been observed in the case of all the remaining compositions too. It is worthwhile to mention that the values of electrical conductivity measured at room temperature (297 K) and represented as $\sigma_{297\,K}$ for the various compositions of the mixed system $(1-x)\cdot CuI$–$x\cdot Ag_2MoO_4$ for $x = 0.15$, 0.2, 0.25, 0.3,0.33, 0.35, 0.4, 0.45, 0.5, 0.55 and 0.6 are 5.5×10^{-7}, 2×10^{-6}, 4.5×10^{-6}, 7.6×10^{-6}, 1.2×10^{-5}, 1.3×10^{-5}, 1.7×10^{-5}, 2.1×10^{-5}, 1.2×10^{-4}, 1.5×10^{-3} and $3.2\times10^{-4}\,S\,cm^{-1}$, respectively. This implies that the best conducting compositions may be considered as the specimen having $x = 0.55$ in Series II of the chosen system. It is well known that pure γ-CuI exhibits a room temperature conductivity of the order of $10^{-7}\,S\,cm^{-1}$, whereas γ-AgI possesses an electrical conductivity of $10^{-6}\,S\,cm^{-1}$ at ambient temperatures [22,23]. Accordingly, the gradual increase in the observed room temperature conductivity from 5.5×10^{-7} to $1.2\times10^{-5}\,S\,cm^{-1}$ when x is increased from 0.15 to 0.33 may be attributed to the formation of $Cu_{1-a}Ag_aI$ type solid solutions as possible constituents of these compositions. These results are found to be in good agreement with those obtained during the present XRD and DSC studies. Similarly, in the case of various compositions of Series II, the observed room temperature electrical conductivity values lie in the range of 10^{-5}–$10^{-3}\,S\,cm^{-1}$. These values may be attributed to the presence of AgI formed due to the solid-state reaction and Ag_2MoO_4 (excess) in these specimens as revealed by Eqs. (7)–(12). The occurrence of appreciably high electrical conductivity values of $1.5\times10^{-3}\,S\,cm^{-1}$ in the case of $x = 0.55$ may be explained on the basis of the temperature-dependant electrical conductivity and ionic transport number data presented in the following section.

3.4.1. Temperature-dependant conductivity and transport number data

Fig. 10 shows the plots of $\log\sigma T$ versus $1000/T$ obtained for the five different compositions in Series I of the mixed system $(1-x)\cdot CuI$–$x\cdot Ag_2MoO_4$ containing $x = 0.15$, 0.2, 0.25, 0.3 and 0.33 in the temperature range 297–447 K. On the other hand, Fig. 11 depicts the plots of $\log\sigma T$ versus $1000/T$ observed for the various compositions having $x = 0.35$, 0.4, 0.45, 0.5, 0.55 and 0.6 in Series II over the above temperature range. It is seen from Fig. 10 that among the various compositions in Series I, the particular sample having $x = 0.33$ shows a second-order phase transition at around 420 K, while all those samples are found to obey the Arrhenius behavior over the above temperature range of investigation. The fact that most of the specimens of Series II of the mixed system $(1-x)\cdot CuI$–$x\cdot Ag_2MoO_4$ show a second-order phase transition at around 420 K is also evident from Fig. 11, apart from their Arrhenius behavior with temperature. The set of activation energies (E_a) estimated from the relationship

$$\sigma = (\sigma_0/T)\exp(-E_a/kT) \qquad (13)$$

(where k denotes the Boltzman constant, T the absolute temperature and σ_0 the 'pre-exponential factor') are

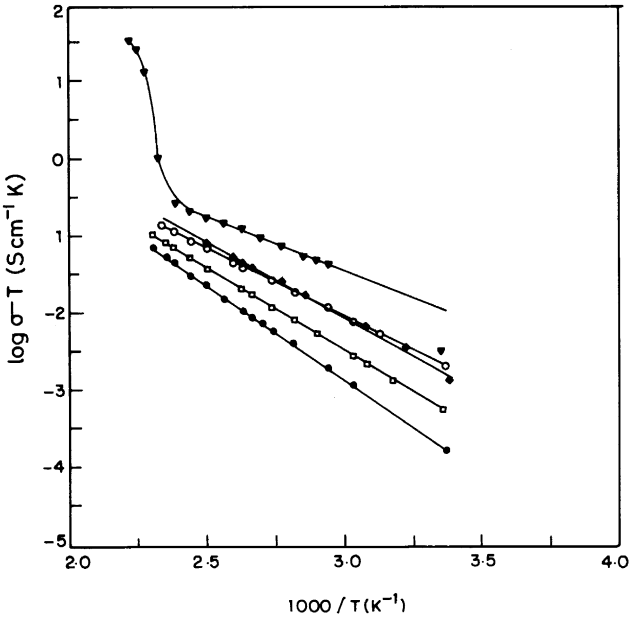

Fig. 10. Plots of $\log\sigma T$ versus $1000/T$ for samples in Series I: $x = 0.15$ (●); $x = 0.2$ (□); $x = 0.25$ (◆); $x = 0.3$ (○) and $x = 0.33$ (▼).

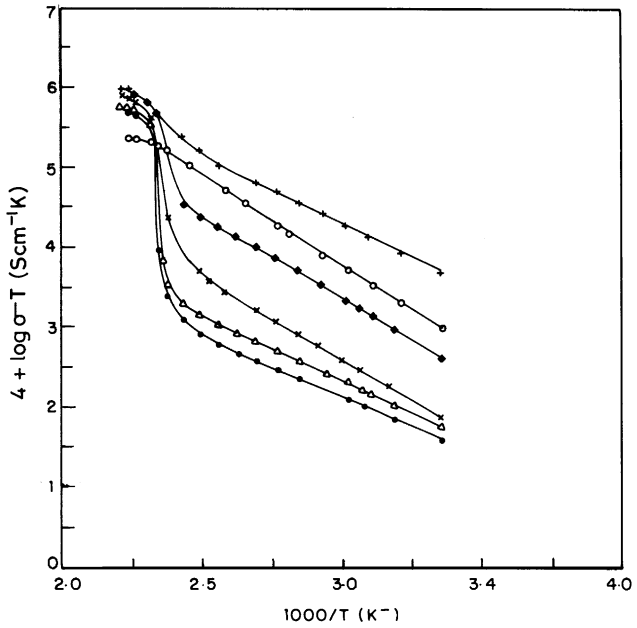

Fig. 11. Plots of $\log \sigma T$ versus $1000/T$ for samples in Series II: $x = 0.35$ (●); $x = 0.4$ (△); $x = 0.45$ (×); $x = 0.5$ (◆); $x = 0.55$ (+) and $x = 0.6$ (○).

Table 2
The values activation energies for effective electrical conduction and associated ionic transport number data for various compositions in the mixed system $(1-x)\cdot CuI - x\cdot Ag_2MoO_4$ ($0.15 \leqslant x \leqslant 0.6$)

Composition, X	Activation energy, E_a (eV)	Ionic transport number, t_i
0.15	0.49	0.47
0.2	0.42	0.84
0.25	0.38	0.94
0.3	0.35	0.94
0.33	0.29	0.98
0.35	0.3	0.97
0.4	0.32	0.97
0.45	0.42	0.97
0.5	0.43	0.98
0.55	0.36	0.98
0.6	0.41	0.98

presented in Table 2 together with the corresponding composition and room temperature transport number (t_i) data obtained during the present investigation. It is clear from Table 2 that the activation energies lie in the region 0.29–0.49 eV. The observed ionic transport number values in the case of Series I vary from 0.47–0.98 when x is increased from 0.15 to 0.33 where as in the case of Series II, the value of 't_i' is almost constant, i.e., 0.97–0.98 at ambient temperature.

The appearance of the second-order transition at around 420 K in the plot of $\log \sigma T$ versus $1000/T$ in Fig. 10 is comparable to the $\beta \rightarrow \alpha$ phase transition temperature of AgI observed at 423 K in the DSC thermograms for the particular composition corresponding to $x = 0.33$ in Series I of the mixed system under investigation. In other words, the observed electrical conductivity of $1.2 \times 10^{-5}\,S\,cm^{-1}$ in the case of $x = 0.33$ and the corresponding ionic transport number of 0.98 appear to reveal the feasibility of obtaining silver ionic conduction in the sample as in the case of pure AgI [23]. However, the relatively lower t_i values of 0.47, 0.84, 0.94 and 0.94 noticed in the case of $x = 0.15$, 0.2, 0.25 and 0.3 may be attributed to the mixed ionic/electronic transport within such composition. Furthermore, the ionic transport number is found to increase from a relatively low value of 0.47 to as high as 0.98, whereas the corresponding activation energy for effective electrical transport is found to decrease from 0.49 to 0.29 eV when x is increased from 0.15 to 0.33. These features appear to suggest that the resultant solid solution $Cu_{1-a}Ag_aI$ ($0 \leqslant a \leqslant 1$) formed due to the solid-state reaction between CuI and Ag_2MoO_4 as outlined by Eqs. (2)–(6) may be the probable source of mobile ion in Series I of the mixed system. This argument is further supported by the fact that the typical $Cu_{1-a}Ag_aI$ solid solution having 47 mol% of AgI was reported to behave as a pure silver ionic conductor [24,25].

On the other hand, in the case of Series II, it is interesting to note from Fig. 11 that the appearances of the second-order phase transition temperatures at around 420 K in different samples having $x = 0.35$, 0.4, 0.45, 0.5 and 0.55 may be compared to the typical endothermic transitions observed at 423, 423, 421, 420 and 420 K in the corresponding DSC thermograms as described earlier. It is therefore clear that all the peaks may be due to the presence of AgI as one of the reaction products in these compositions in accordance with the proposed solid-state reactions (Eqs. (7)–(12)). It is clear from Table 2 that all the six different compositions of Series II are ionic in nature, exhibiting ionic transport number values of 0.97–0.98 at ambient temperature. The fact that the observed electrical conductivity values are the order of 10^{-5}–$10^{-3}\,S\,cm^{-1}$ in the case of specimens of Series II shows that AgI may be responsible for these values. It is already obvious from Eqs. (7)–(12) that AgI is present in all these samples, thus indicating the feasibility of silver ionic conduction in such compositions. A comparison of the room temperature electrical conductivity value of $1.5 \times 10^{-3}\,S\,cm^{-1}$ observed for the best conducting specimen having $x = 0.55$ with the corresponding value of $1.2 \times 10^{-5}\,S\,cm^{-1}$ found for the composition with $x = 0.33$ tend to suggest that the higher conductivity of the former may be associated with the presence of Ag_2MoO_4 (excess) thus providing a more disordered structure as compared to the latter, in accordance with the XRD results as well as Eqs. (6)–(11).

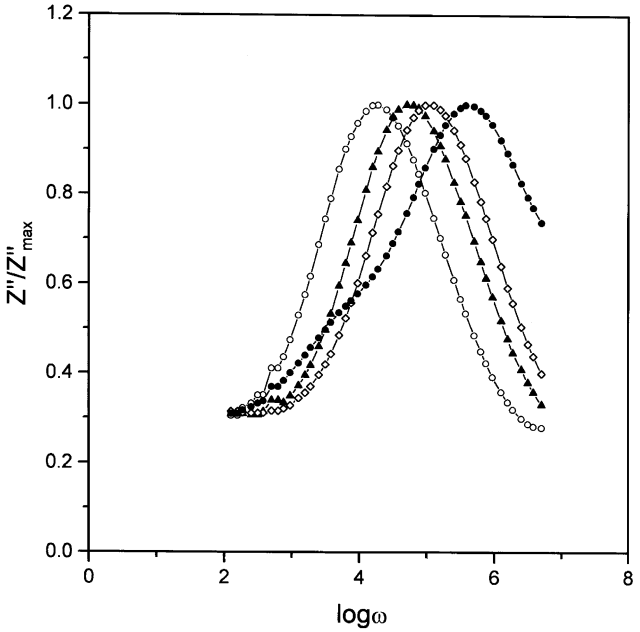

Fig. 12. Normalized impedance spectra obtained for the sample having $x = 0.55$ at different temperatures: T = 297 K (○); 330 K (▲): 380 K (△) and 425 K (●).

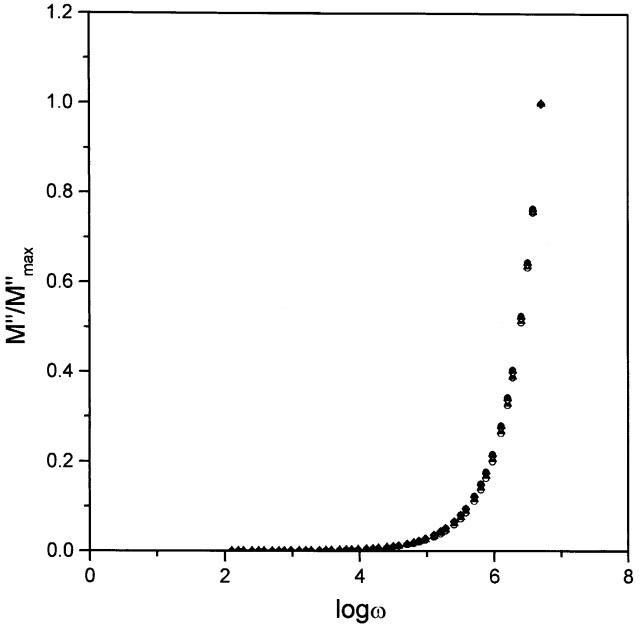

Fig. 13. Normalized modulus spectra obtained for the sample having $x = 0.55$ at different temperatures: $T = 297$ K (○); 330 K (▲): 380 K (◇) and 425 K (●).

In the case of various specimens in Series II of the present mixed system, it is seen that the observed ionic transport number values lie in the region 0.97–0.98. This means that the remaining 2–3% of contribution to the total conductivity may be electronic in nature. The origin of electronic conductivity in these samples may be visualized in terms of the presence of metallic silver in these cases. The formation of traces of metallic silver has already been identified in the various specimens of Series II. However, the deviation of the observed t_i values from unity in the case of samples having $x = 0.15$, 0.2, 0.25 and 0.3 may be attributed to the mixed conduction involving electronic and/or Cu^+ ionic contribution.

3.4.2. *Impedance and modulus spectra*

It is obvious from the preceding section that the best conducting composition of the mixed system $(1-x)\cdot CuI–x\cdot Ag_2MoO_4$, namely $0.45CuI–0.55Ag_2MoO_4$ would exhibit an electrical conductivity of $1.5\times10^{-3}\,S\,cm^{-1}$ at 297 K. In order to understand the conductivity behavior as a function of frequency and to identify and separate the various electrode and grain-boundary effects from the observed features of the bulk specimen corresponding to the above composition, temperature-dependant complex impedance and spectra have been drawn. Fig. 12 shows the normalized impedance spectra (Z''/Z''_{max} versus $\log\omega$) obtained for the sample having $x = 0.55$ at four different temperatures, viz., 297, 330, 380 and 425 K, respectively. On the other hand, Fig. 13 shows the normalized modulus spectra (M''/M''_{max} versus $\log\omega$) obtained for the above sample at 297, 330, 380 and 425 K, respectively. In Fig. 12, the observed shift in the high-frequency peak corresponding to the bulk property of the sample towards higher frequencies with increase in temperature suggests that the bulk relaxation is a function of temperature and would occur at higher frequencies at elevated temperatures. From Fig. 13 it is seen that the modulus curves observed at different temperatures are super impossible and that the bulk property alone is noticed in the high-frequency region. The observed broad nature of the modulus spectrum may be considered as due to the summation of different peaks separated from each other by at least an order of magnitude on the frequency scale. As a result, the peaks in the impedance and modulus spectra would occur at different frequencies, the impedance spectrum being narrower than the corresponding modulus spectrum. It is also worthwhile to mention that the long tail seen at lower frequencies in the modulus spectra may be attributed to the larger capacitance associated with the electrodes [26]. The non-perturbed shape of the modulus spectra at different temperatures clearly signifies the temperature independence of the distribution of relaxation times (DRT), in view of the multi-phase heterogeneous nature of the present system $CuI–Ag_2MoO_4$. The physical significance of the temperature independent DRT is that the distribution of conductivities in the specimen due to the various layers within the solid is temperature independent [27].

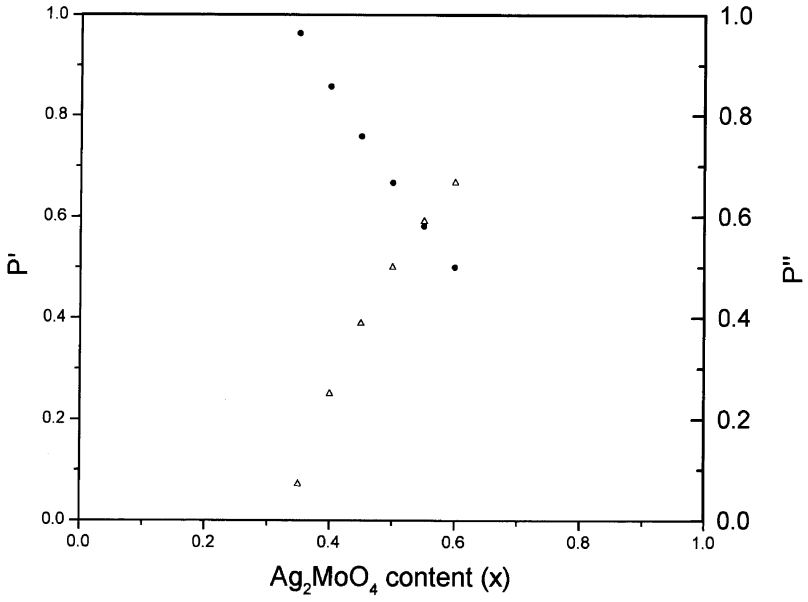

Fig. 14. Relative strengths of AgI (P') and Ag_2MoO_4 (P'') as a function of composition (x): P' (●) and P'' (△).

3.4.3. Possible role of oxysalts in the effective electric conduction of the mixed system

In the case of AgI–Ag oxysalt systems, the composition dependence of room temperature electrical conductivity was reported to be linear with respect to the total mole fraction of AgI present [28,29]. As the above approach considered only those Ag^+ ions originating from the dissociation of AgI as the mobile charge carriers, the relative strength of AgI in the mixture of AgI–Cu_2MoO_4–Ag_2MoO_4 (excess) may be defined as

$$P' = \frac{\text{AgI}}{\text{AgI} + \text{Ag}_2\text{MoO}_4\ (\text{excess})} \tag{14}$$

and treated as a composition variable in the case of Series II. As a consequence, the presence of Cu_2MoO_4 and Ag_2MoO_4 (excess) would be expected to have insignificant influence on the migration pathways of Ag^+ ions in this system. However, the large deviation in the value of observed conductivity for the composition with $x = 0.55$ from that of the remaining compositions tends to suggest that the oxyanion framework may also play a significant role in the effective electric conduction phenomena. Under normal conditions, it may be suggested that the presence of Cu_2MoO_4 would suppress the effect of Ag_2MoO_4 (excess). Accordingly, in the typical sample having $x = 0.5$, where the concentration of both these oxysalts are equal the resulting effect would be that of AgI only. However, the observed conductivity of $1.2 \times 10^{-4}\,\text{S cm}^{-1}$which is higher than that of γ-AgI may be attributed to the combined effects of Cu_2MoO_4 and Ag_2MoO_4 (excess) within the mixture. Predictably, the formation of possible equilibrium phases at a particular temperature may be controlled by the concentration of two types of oxyanion salts present, viz., Cu_2MoO_4 and Ag_2MoO_4 (excess) and hence the relative strength of Ag_2MoO_4 (excess) may be expressed as

$$P'' = \frac{\text{Ag}_2\text{MoO}_4\ (\text{excess})}{\text{Cu}_2\text{MoO}_4 + \text{Ag}_2\text{MoO}_4\ (\text{excess})}. \tag{15}$$

Fig. 14 depicts the plots of P' and P'' as a function of Ag_2MoO_4 content (x) within the different specimens of the mixed system $(1-x)\cdot\text{CuI}$–$x\cdot\text{Ag}_2\text{MoO}_4$. It is interesting to note from Fig. 14 that these two plots cross at the typical value corresponding to $x = 0.55$, which is found to be the best conducting composition of the present system. It is therefore, apparent from the above discussion that the oxyanion salts such as Cu_2MoO_4 and Ag_2MoO_4 (excess) may also influence of the system as is evident on the basis of the most probable solid-state reactions involved.

4. Conclusion

The present XRD, DSC and FT-IR results obtained for the mixed system $(1-x)\cdot\text{CuI}$–$x\cdot\text{Ag}_2\text{MoO}_4$ have revealed the formation of solid solutions of the type $Cu_{1-a}Ag_aI$ ($0 \leqslant a \leqslant 1$) and Cu_2MoO_4 as probable reaction products during melting where $x = 0.15$, 0.2, 0.25, 0.3 and 0.33, respectively, whereas solid phases including AgI, Cu_2MoO_4 and Ag_2MoO_4 appear to constitute those compositions involving $x = 0.33$, 0.35, 0.4, 0.45, 0.5, 0.55 and 0.6. Further investigations concerning complex impedance analysis and ionic transport measurements have suggested that the best conducting composition having $x = 0.55$ would exhibit an electrical conductivity of $1.5 \times 10^{-3}\,\text{S cm}^{-1}$ at 297 K due to silver

ionic transport. A series of solid-state reactions proposed for all the various compositions of the chosen system appear to substantiate the observed features.

Acknowledgments

The authors are grateful to the University Grants Commission, New Delhi for the financial assistance offered in the form of a research award project (No.F.30-65/98/SA-III).

References

[1] M.Z.A. Munshi, Handbook of Solid State Batteries and Capacitors, World Scientific, Singapore, 1995.
[2] S.A. Suthanthiraraj, S. Murugesan, P. Maruthamuthu, Solid State Ionics 143 (2001) 413.
[3] S.A. Suthanthiraraj, R. Mala, Solid State Ionics 144 (2001) 143.
[4] S.A. Suthanthiraraj, S. Murugesan, P. Maruthamuthu, Solid State Ionics 130 (2000) 299.
[5] V.G. Chandrasekhar, S.A. Suthanthiraraj, J. Mater. Sci. 28 (1993) 4043.
[6] A. Viswanathan, S.A. Suthanthiraraj, Solid State Ionics 58 (1992) 89.
[7] N.M. Tallan, H.C. Graham, J.M. Wimmer, Mater. Sci. Res. 3 (1996) 111.
[8] G. Burley, Am. Mineral 48 (1963) 1266.
[9] J.R. Macdonald, J. Electroanal. Chem. 53 (1974) 1.
[10] J.R. Macdonald, Impedance Spectroscopy, Wiley Interscience, New York, 1987.
[11] J.R. Macdonald, J. Chem. Phys. 61 (1974) 3977.
[12] J.R. Macdonald, J. Chem. Phys. 58 (1973) 4982.
[13] K. Knikkola, C. Wagner, J. Electrochem. Soc. 104 (1957) 379.
[14] J.S. Mckechni, L.D.S. Turner, C.A. Vincent, J. Chem. Thermodyn. 11 (1979) 1189.
[15] T. Takahashi, N. Wakabayashi, O. Yamamoto, J. Solid State Chem. 21 (1977) 73.
[16] E.X. Cox, in: J.D.H. Donnay (Ed.), American Crystallographic Monograph, Crystal data Determinative Tables, Number 5, American Crystallographic Association, Washington DC, 1963, p. 898.
[17] S. Miyake, S. Hoshino, T. Takenaka, J. Phys. Soc. Jpn. 7 (1952) 19.
[18] N. Machida, Y. Shinkuma, T. Minami, Solid State Ionics 45 (1991) 123.
[19] P. Caillet, P. Saumagne, J. Mol. Struct. 4 (1969) 351.
[20] N. Machida, H. Eckert, Solid State Ionics 107 (1998) 255.
[21] W. Jost, Diffusion und Chemische Reaktion in Festen Stoffen, Verlag Von Theodor Steinkopff, 1937.
[22] T. Matsui, J.B. Wagner Jr., J. Electrochem. Soc. 124 (1977) 300.
[23] T. Takahashi, K. Kuwabara, O. Yamamoto, J. Electrochem. Soc. 116 (1977) 357.
[24] J.A. Schmidt, R. Fornari, J.C. Bazan, Electrochim Acta 24 (1979) 1131.
[25] N. Chellamal, N. Gogulamurali, S.A. Suthanthiraraj, P. Maruthamuthu, Bull. Electrochem. 6 (1990) 625.
[26] I.M. Hodge, M.D. Ingram, A.R. West, J. Electroanal. Chem. 74 (1976) 125.
[27] S.W. Martin, C.A. Angell, J. Non-Cryst. Solids 83 (1986) 185.
[28] S.W. Martin, A. Schiraldi, J. Phys. Chem. 89 (1985) 2070.
[29] A. Schiraldi, Electrochim. Acta 23 (1978) 1039.